Sensitizers

International Edition: DOI: 10.1002/anie.201604432
German Edition: DOI: 10.1002/ange.201604432

First-Generation Subporphyrinatoboron(III) Sensitizers Surpass the 10% Power Conversion Efficiency Threshold

Graeme Copley[+], Daesub Hwang[+], Dongho Kim, and Atsuhiro Osuka**

Abstract: *Subporphyrinatoboron(III) (SubB) sensitizers were synthesized for use in dye-sensitized solar cells (DSSCs). The prototype, which comprises a sterically demanding 3,5-di-tert-butylphenyl scaffold, a meso-ethynylphenyl spacer, and a cyanoacrylic acid anchoring group, achieved an open-circuit voltage V_{OC} of 836 mV, short-circuit current density J_{SC} of 15.3 mA cm^{-2}, fill factor of 0.786, and a photon-to-current conversion efficiency of 10.1%. Such astonishing figures suggest that a bright future lies ahead for SubB in the realm of DSSCs.*

The first practical photovoltaic technologies utilized "solar-grade silicon" in p–n junction devices.[1] Although it is possible to achieve power conversion efficiency (PCE) values of greater than 20% with such technologies, the accompanying non-environmentally friendly and high-cost manufacturing processes halted global scale up. These drawbacks encouraged researchers to search for ecofriendly low-cost alternatives. In 1991, O'Regan and Grätzel developed a new photovoltaic cell which operated on the principles of plant photosynthesis.[2] Colloidal TiO_2 films coated with a ruthenium(II)-based dye were used in conjunction with an iodide-based electrolyte to achieve certified PCE values of 7.1 to 7.9%. The term dye-sensitized solar cell (DSSC) was later coined for this setup. The record PCE value achieved by a ruthenium(II)-based DSSC currently stands at 11.9%,[3] but again drawbacks such as the low-earth abundance and high cost of ruthenium make such systems economically infeasible. Going beyond 12% PCE in an economically and environmentally sound manner required another visit to the drawing board.

A new generation of DSSCs which consist of donor–π-acceptor (D-π-A) organic dyes supplemented by cobalt-based redox mediators, as opposed to the classical $I^{3-/1-}$ redox shuttle, have started something of a renaissance.[4–6] These systems maintain a clear lead in the DSSC field, generating PCE values above 11%. Most relevant to this study, the record for porphyrin-based D-π-A sensitizers is currently held by SM315 (PCE ≈ 13%), a push–pull porphyrin dye which was engineered to achieve a wide panchromatic light response and optimal compatibility with the cobalt-based electrolyte.[7,8]

Subporphyrinatoboron(III) (hereinafter referred to SubB), a ring-contracted cousin of porphyrin which houses a central boron atom, has been extensively investigated in our laboratories following its emergence in 2006.[9] SubB singlet excited states bear resemblance to those of porphyrin, emit fluorescence with reasonably high quantum yields, and display single exponential decays with lifetimes on the order of several nanoseconds.[10] Such properties suggest that SubBs are promising candidates for use as molecular sensitizers in DSSCs. In addition, SubBs possess several advantageous attributes. Firstly, SubBs are chemically robust, thus allowing operational longevity. Secondly, SubBs have domed bowl-shaped structures and axial *B*-substituents. Such features should help suppress intermolecular aggregation at the electrode surface, a common culprit known to impede device performance. Thirdly, the meso-aryl substituents of SubB can rotate rather freely, thus giving rise to a wide range of conformer distributions with respect to dihedral angle, and is expected to enhance light-harvesting capabilities. The facile rotation of the meso-aryl substituents is also expected to enhance conjugative interactions between subunits of the dye to facilitate electron injection into the TiO_2 from the photo-excited state of SubB, for example. Encouraged by these features, we decided to develop and test the first generation of SubB-based DSSCs.

The SubB sensitizers examined in this study are depicted in Scheme 1. The prototype **1** is the simplest prototype, with the SubB nucleus bearing tolyl groups (providing slight steric bulk), a simple phenyl bridge and a simple carboxylic acid anchoring group. The prototype **1** was synthesized by following our protocol for synthesizing A_2B-type SubBs.[11] The appropriate tripyrrane was preorganized around $BH_3{\cdot}NEt_3$ in *o*-dichlorbenzene at 150 °C, followed by methyl 4-(chlorocarbonyl)benzoate in the ring-closing step. This protocol afforded the methyl ester analogue of prototype **1**, $\mathbf{1}_{ester}$, in 15% yield. The free carboxylic acid group was quantitatively unmasked under basic conditions. Purification of **1** was far from trivial, as the compound strongly adsorbed on silica gel. Furthermore, the free carboxylic acid group can associate with the central boron atom of neighboring SubBs in solution, thus leading to the formation of random molecular assemblies. This behavior was previously encountered for an A_2B-type SubB bearing an ethynylbenzene spacer terminated by a 2-carboxyphenyl group, and had the tendency to form a complementary face-to-face dimer in solution.[12] When

[*] Dr. G. Copley,[+] Prof. Dr. A. Osuka
Department of Chemistry, Graduate School of Science
Kyoto University
Sakyo-ku Kyoto, 606-8502 (Japan)
E-mail: osuka@kuchem.kyoto-u.ac.jp
D. Hwang,[+] Prof. Dr. D. Kim
Spectroscopy Laboratory for Functional π-Electronic Systems and
Department of Chemistry, Yonsei University
Seoul 120-749 (Korea)
E-mail: dongho@yonsei.ac.kr
[+] These authors contributed equally to this work.

Supporting information for this article can be found under: http://dx.doi.org/10.1002/anie.201604432.

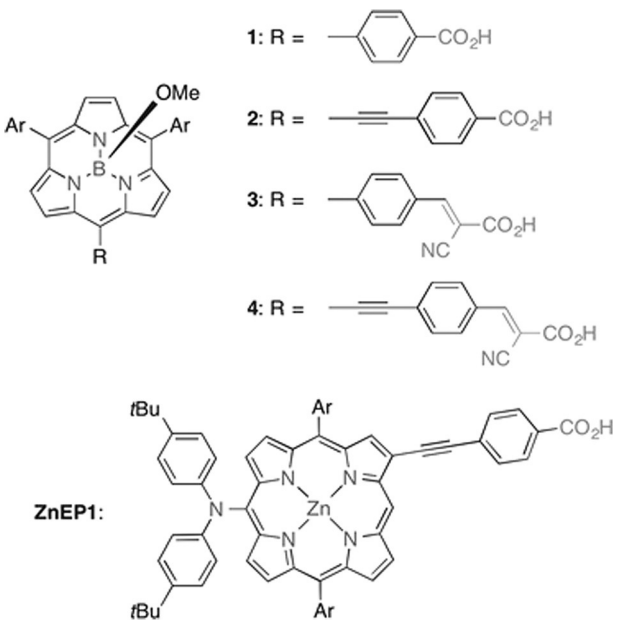

Scheme 1. SubB sensitizers **1**–**4** and control porphyrin **ZnEP1** investigated in this study. Ar = 4-tolyl for **1**–**3**, Ar = 3,5-di-*tert*-butylphenyl for **4**, and Ar = 4-*tert*-butylphenyl for **ZnEP1**.

thin-layer chromatography (TLC) confirmed complete consumption of the starting ester, the reaction mixture was carefully acidified to pH 3–5 using 1M HCl. CH_2Cl_2 was then used for extraction followed by standard work-up procedures. It is essential that the resulting crude material is subjected to axial exchange heating cycles in a 1:1 mixture of CH_2Cl_2/MeOH (1 cycle = 50 °C for ≈15 min) to break up and suppress the undesired formation of molecular assemblies by forcefully converting all of the boron axial ligands into the methoxy group. Finally, recrystallization from CH_2Cl_2/MeOH, followed by repeated washes with *n*-hexane yielded **1** in ultra-pure form. The purification steps outlined above can be applied to the other prototypes described in this study.

The prototypes **2**, **3**, and **4** were all accessed from the A_2B-type meso-bromo-SubB platform reported previously by our group (in the case of **4**, a custom-made 3,5-di-*tert*-butylphenyl scaffold was employed).[13] The prototype **2**, similar in structure to prototype **1**, additionally incorporates an acetylene spacer which was intended to red-shift its absorption profile, to boost light harvesting capabilities, and to enhance the conjugative interaction between the SubB chromophore and anchoring arm. The prototype **2** was prepared by reacting the appropriate meso-bromo-SubB with methyl 4-ethynylbenzoate under classical Sonogashira conditions to yield the methyl ester $\mathbf{2}_{ester}$. Basic ester hydrolysis was again used to unmask the free carboxylic acid group to furnish **2** quantitatively. The prototype **3** was intended to test a new anchoring moiety, namely the cyanoacrylic acid group. We choose the cyanoacrylic acid anchoring group as it seemed to be a prevalent and effective choice in the literature.[14] The prototype **4** is a marriage of prototypes **1**–**3**, and possesses two 3,5-di-*tert*-butyl-phenyl groups to increase steric bulk, an attribute that was envisaged to enhance dye-loading capabilities and suppress undesired intermolecular aggregation at the electrode surface. For the synthesis of **3** and **4**, Knoevenagel condensations (cyanoacetic acid with ammonium acetate catalyst) were carried out on the corresponding formyl-substituted SubBs to furnish the *E*-isomer products stereoselectively. The structures of the methyl esters $\mathbf{1}_{ester}$ and $\mathbf{2}_{ester}$ were confirmed by single-crystal X-ray diffraction analysis (see Figure S6 in the Supporting Information).

The absorption spectra of **1**–**4**, along with the control porphyrin **ZnEP1**, were recorded for samples loaded onto TiO_2 (Figure 1). This step was to eradicate any broadening of

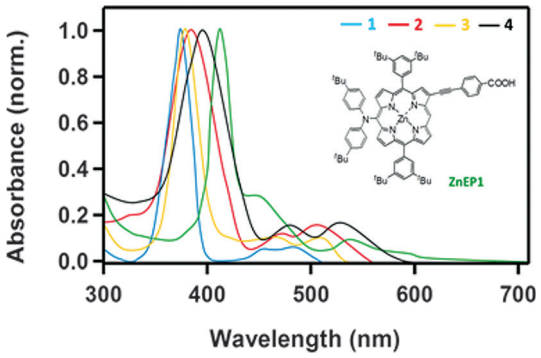

Figure 1. Absorption spectra of **1**–**4** and **ZnEP1** loaded on TiO_2.

the absorption profiles resulting from boron-acid-induced aggregation. Table 1 contains a summary of the photophysical properties of **1**–**4**. The absorption spectra of **1**–**4**, and $\mathbf{1}_{ester}$–$\mathbf{4}_{ester}$ were also recorded in CH_2Cl_2 (in the case of **4**, the absorption spectrum was recorded in MeOH to reduce broadening effects; see Figures S5–S8).

Table 1: Photophysical parameters of **1**–**4** in solution and loaded onto TiO_2.[a]

Cmpd	ε [$M^{-1}cm^{-1}$][b]	λ_{max} [nm][c]	λ_{em} [nm][d]	Φ_F[e]
1	87000	376, 462, 489 (371, 456, 487)	532	0.14
2	93000	392, 512 (385, 474, 513)	538	0.23
3	79000	381, 468, 502 (376, 469, 512)	561	0.18
4	100000	395, 515 (398, 483, 535)	541	0.33

[a] Values within the parentheses indicate the peak positions for samples loaded onto TiO_2. Data of **1**–**3** recorded in CH_2Cl_2. Data for **4** measured in MeOH. [b] Molar extinction coefficient. [c] Soret and Q band peak maxima. [d] The wavelength of maximum emission following excitation at the Soret wavelength. [e] Fluorescence quantum yield.

Two essential prerequisites for a dye to function in a DSSC are that the HOMO level (first oxidation potential) of the dye lies below that of the potential of the redox mediator (in our case E [$Co(bpy)_3$]$^{n+}$ ≈ +0.57 V vs. NHE) and the LUMO sits above the conduction band of the TiO_2 (≈ −0.5 V vs. NHE). Determination of the oxidizing power of the excited state of the dye can be roughly calculated by subtracting the $E_{0\text{-}0}$ energy (estimated from the intersection of

Table 2: Redox potentials of **1e–4e**.[a]

Cmpd	$E_{1/2OX}$[b] [V]	$E_{1/2RED}$[c] [V]	$E_{0\text{-}0}$[d] [eV]	E_{OX^*}[e] [V]	ΔG_{INJ}[f] [eV]	ΔG_{CR}[g] [eV]
$\mathbf{1}_{ester}$	1.48	−1.12	2.51	−1.03	−0.53	−1.98
$\mathbf{2}_{ester}$	1.31	−1.09	2.42	−1.11	−0.61	−1.81
$\mathbf{3}_{ester}$	1.38	−1.17	2.38	−1.00	−0.5	−1.88
$\mathbf{4}_{ester}$	1.28	−1.32	2.28	−1.00	−0.5	−1.78

[a] Values were determined by cyclic voltammetry. Conditions: scan rate: 0.05 Vs^{-1}, supporting electrolyte: 0.1 M nBu_4NPF_6, working/counter electrodes: Pt/Pt wire, reference electrode: Ag/0.01 M $AgClO_4$ in CH_2Cl_2. Recorded values have been adjusted/referenced to NHE for convenience. [b] First oxidation potential of the SubB core. [c] First reduction potential of the SubB core. [d] Zero-zero energy estimated from the intersection of absorption and emission spectra. [e] Excited-state oxidation potentials estimated from $E_{1/2OX}$ and $E_{0\text{-}0}$. [f] Driving force for electron injection from the SubB first excited singlet state in to the conduction band of TiO_2. [g] Driving force for charge recombination from the conduction band of TiO_2 to the SubB radical cation.

the absorption and emission spectra) from the HOMO level of the dye. Electrochemical characterization of $\mathbf{1}_{ester}$–$\mathbf{4}_{ester}$ was performed in CH_2Cl_2. Table 2 contains a summary of the electrochemical data.

It is quite clear that replacement of the phenyl bridge with an acetylene bridge at the meso-position of SubB has a significant impact on the first oxidation potential. This impact is likely due to the low dihedral angle with respect to the SubB core and acetylene unit (just 9°) and electron-donating nature of the acetylene unit. The electron-donating 3,5-di-*tert*-butylphenyl groups significantly elevate the reduction potential of the SubB core of $\mathbf{4}_{ester}$. The electrochemical data are in good agreement with the MO diagrams calculated for $\mathbf{1}_{ester}$–$\mathbf{4}_{ester}$ (see Figure S8).

The total amount of the SubB dyes adsorbed onto the TiO_2 layers (Γ, mol cm^{-2}) was determined by Langmuir adsorption isotherm plots.[15] To investigate the dye-loading process, the UV-vis absorption spectra of the five dyes adsorbed onto TiO_2 spheres were acquired (Figure 1). The amount of adsorbed dye can be calculated by using the extinction coefficients of **1**, **2**, **3**, **4**, and **ZnEP1** dye (0.87×10^7, 0.93×10^7, 0.79×10^7, 1×10^7, and 1.6×10^7 $mol^{-1}cm^2$, respectively). Figure S11 shows the plots for the absorbance versus the dye loading time. The dyes **1**–**4** were adsorbed rapidly in just a few hours, with the adsorption process slowing down upon approaching saturation. The dye **4** displayed a much higher (ca. 3 times) dye-loading saturation level ($>20\times10^{-9}$ mol cm^{-2}) than **ZnEP1** (ca. 7×10^{-9} mol cm^{-2}). The adsorption process can be described using the following equation: $-(d(1-\theta)/dt)=\kappa(1-\theta)^n$, where θ is the dye coverage, κ represents the reaction constant, and n is the reaction order.[16] The inset in Figure S11-1 shows the fitting result with $n=1$, where $\ln(1-\theta)$ exhibited a linear dependence on the dye-loading time, t. From this fitting the reaction constants κ were calculated to be 0.34 min^{-1} for **1**, 0.70 min^{-1} for **2**, 0.36 min^{-1} for **3**, 2.8 min^{-1} for **4**, and 0.13 min^{-1} for **ZnEP1**. The calculated κ value for the **4**-based photoelectrode was approximately 20 times higher than that of the **ZnEP1**-based photoelectrode.

To highlight the impact of the larger molar extinction coefficient and higher dye loading of the SubB sensitizers, we have fabricated TiO_2 sphere-based electrodes with CDCA in a 1:1 ratio of dye/CDCA (5×10^{-4} M/5×10^{-4} M). **ZnEP1** was used as a reference dye. The current density-voltage (J–V) characteristics and incident photon-to-current efficiencies (IPCE) spectra of the SubB based DSSCs are shown in Figure 2, from which open-circuit photovoltage (V_{oc}), short-

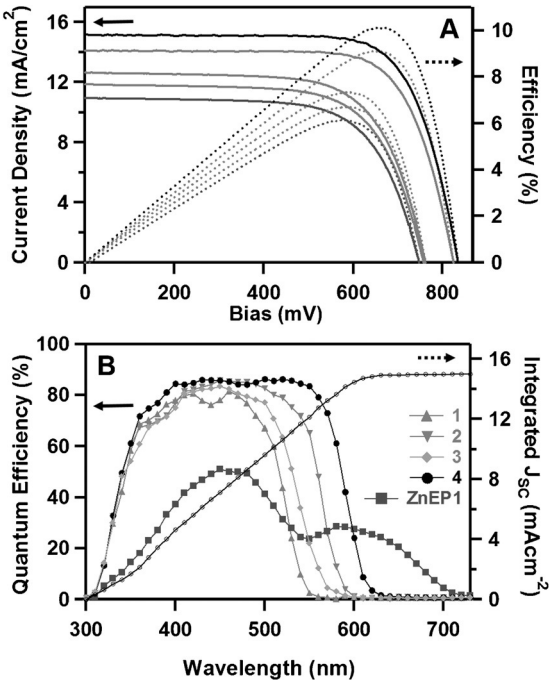

Figure 2. A) Current-voltage characteristics and B) action spectra at incident photon-to-current efficiencies (IPCE) and integrated photocurrent density (J_{sc}) of SubB and Zn-porphyrin-sensitized solar cells. Conditions: $[Co(bpy)_3]^{2+/3+}$-based electrolyte in CH_3CN and AM 1.5 under simulated solar light irradiation (99.8 mW cm^{-2}).

circuit photocurrent density (J_{sc}), fill factor (FF), and photon-to-current conversion efficiency (PCE) were determined (Table 3). Direct comparison of the performance of the DSSCs were conducted for the electrodes with the same thickness (ca. 7 μm) and indicates higher efficiencies of **1**–**4** than that of **ZnEP1**. While DSSCs using **1** and **3**, beairng a meso-phenyl bridge, exhibited similar *V*oc and J_{SC} values, those using **2** and **4**, bearing an acetylene bridge, displayed

Table 3: Summary of photovoltaic performance of SubB- and **ZnEP1**-sensitized solar cells.

Cmpd	V_{oc}[a] [mV]	J_{sc}[b] [mA cm^{-2}]	FF[c] [%]	PCE[d] [%]
1	760 ± 3	11.8 ± 0.3	74.4 ± 0.5	6.7 ± 0.2
2	823 ± 3	14.4 ± 0.2	77.9 ± 0.2	9.2 ± 0.1
3	763 ± 5	12.6 ± 0.5	75.3 ± 0.3	7.3 ± 0.3
4	836 ± 2	15.3 ± 0.3	78.6 ± 0.2	10.1 ± 0.2
ZnEP1	747 ± 4	10.9 ± 0.4	73.2 ± 0.3	6.0 ± 0.3

[a] Open-circuit voltage. [b] Short-circuit current. [c] Fill factor. [d] Solar to electric power conversion efficiency.

much larger V_{oc} and J_{SC} values, hence larger PCE values. These results have been ascribed to enhanced light harvesting by **2** and **4**, since their absorption spectra are red-shifted and their absorbances are larger than those of **1** and **3**. Accordingly, **1**, **2**, **3**, and **4** achieved PCE values of 6.7, 9.2, 7.3, and 10.1 %, respectively.

The IPCE values are plotted against excitation wavelengths in Figure 2B. Relatively high plateaus were observed for the IPCE spectra of the cells based on **1**–**4**, with their edges being distinctly red-shifted in the order **1** < **3** < **2** < **4**. These results are consistent with the absorption spectra displayed in Figure 1. The maximum IPCE values were 81 % at $\lambda = 460$ nm for **1**, 84 % at $\lambda = 470$ nm for **2**, 83 % at $\lambda = 450$ nm for **3**, and 86 % at $\lambda = 520$ nm for **4**, whilst that of **ZnEP1** was lower, being 54 % at $\lambda = 450$ nm at most, but spread over a wider range of wavelength. Smaller IPCE values of **ZnEP1** were presumably due to lower dye loading on the TiO_2 surface. The integrated J_{SC} value (14.97 mA cm^{-1}) based on IPCE data were found to be consistent with the J_{SC} value (15.3 mA cm^{-1}) obtained from a solar simulator. This result shows that a spectral mismatch between the simulator and the AM 1.5 standard solar spectrum is negligible.

The enhanced J_{sc} and IPCE values for **1**–**4** as compared with **ZnEP1** were further examined by intensity-modulated photocurrent/photovoltage spectroscopy (IMPS/IMVS; see Figure S12). The photocurrent density of DSSCs is determined by the efficiencies of 1) light harvesting, 2) charge injection, 3) regeneration, and 4) charge collection (η_{cc}).[17] Assuming that the charge injection efficiency from SubB and **ZnEP1** to the electron-transport layer is near unity because of a strong fluorescence quenching phenomenon, J_{SC} and IPCEs depend on light-harvesting, regeneration, and charge collection efficiencies. The light-harvesting efficiency is a strong function of the dye loading, which in turn is correlated to the dye-uptake obtained from Langmuir adsorption isotherm plot as shown in Figure S11-1. The regeneration efficiencies of **2**- and **4**-based solar cells were higher than that of a **ZnEP1**-based solar cell as explained and shown in Figure S13-2. Furthermore, the η_{cc} of DSSCs is determined by the relationship: $\eta_{cc} = 1-(c\,L^2 D^{-1} \tau_R{}^{-1})$ where c is a constant, L is the film thickness of the photoelectrode, D is the diffusion coefficient, and τ_R is the charge recombination lifetime.[18] As shown in the results of charge transport time (τ_{CT}) and D as a function of the incident light intensity in Figure S12-1 and S12-2, the τ_{CT} and D values of the SubB-based solar cells were similar to those of the **ZnEP1**-based solar cell, because the charge-transport time is intrinsic to the used identical photoelectrodes. In contrast, the τ_R values of the cells based on **2** and **4** were approximately five times larger than that of the **ZnEP1**-based cell at an incident photon flux of 3.18×10^{18} cm^2 s^{-1} (Figure 3). Therefore, the η_{cc} value of the **4**-based cell was thus determined to be about 4.7 times higher than that of the **ZnEP1**-based cell because of the significantly long τ_R. The superior charge-collection efficiency coupled with the higher dye loading thus leads to the enhanced J_{SC} and IPCE values in the **4**-based DSSC.

Furthermore, the improvement of the electron density in the TiO_2 conduction band can shift the TiO_2 quasi-Fermi level to more negative potentials, which increases the V_{OC} value.

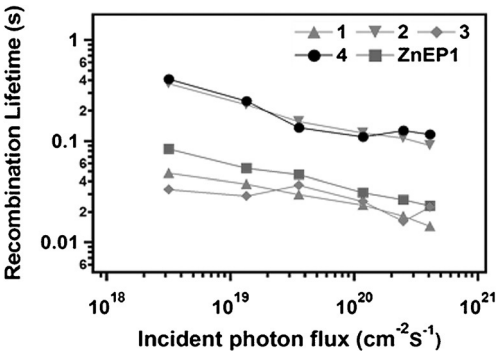

Figure 3. Evolution of charge recombination lifetime of solar cells based on **1**–**4** and **ZnEP1** as a function of incident photon flux measured by frequency-resolved techniques; IMVS results.

Therefore, the V_{OC} value is significantly influenced by τ_R on the TiO_2. The photoelectron density (PED, n) of the DSSC was obtained by the equation: $n = q\,\varphi\,I_0\,\tau_R/q\,(1\text{-}p)d$; where q is the charge of an electron, φ is the ratio of injected electrons to incident photons, I_0 is the incident photon flux density, p is the film porosity, and d is the film thickness.[19] At open-circuit conditions, the recombination current density (J_R) is in proportion to the electron injection current density (J_{inj}). Because J_R and J_{inj} cannot be measured directly, they can be determined from the measurements of the short-circuit photocurrent density (J_{SC}) and the quantum efficiency of injected carriers (α): $q\,\varphi\,I_0 = J_{inj} = J_{SC}/\alpha = -J_R$.[20] Based on this relationship, the PED of the TiO_2 conduction band is proportional to the values of J_{SC} and τ_R. Therefore, the PEDs of the cells based on **2** and **4** were estimated to be more than six times higher than that of the cell based on **ZnEP1**, and can increase the V_{OC} value by about 70 mV. The values of total series resistances were 13 Ω for **4** and 20 Ω for **ZnEP1** as shown in Figure S13-2. The electrochemical data are in good agreement with the values of fill factors as shown in Table 3.

In summary, SubB-based molecular sensitizers **1**–**4** were designed and synthesized for use in DSSCs. The most advanced molecular sensitizer, **4**, was rationally engineered by incorporating the successful design elements of **1**–**3**. The prototype **4** achieved a power conversion efficiency of 10.1 %, which is an astonishing figure for the very first trial of an organic dye. It may be inferred that larger dye loading of **1**–**4** on to TiO_2 layers with respect to **ZnEP1** is a result of SubBs domed structure and axial B-substituent. Numerous avenues remain unexplored, such as improving panchromatic response and functionalizing the central boron atom with either electron-donating or bulky substituents. Removing the boron atom from the central cavity of SubpB(III) remains a significant challenge. However, once this obstacle is overcome the study of sensitizers centered around free-base [14]triphyrin (sub-porphyrin) and sub-porphyrins which house alternative atoms can be explored. The exploration of more advanced SubB-based molecular sensitizers is an active area of research in our laboratories.

Acknowledgments

The work at Kyoto was supported by JSPS KAKENHI grant numbers 25220802 and 25620031. The work at Yonsei was supported by the Global Research Laboratory through the National Research Foundation of Korea (NRF) (2013K1A1A2A02050183) funded by the Ministry of Science, ICT (Information and Communication Technologies). G.C. thanks JSPS for postdoctoral fellowship.

Keywords: boron · dyes/pigments · macrocycles · sensitizers · solar cells

How to cite: *Angew. Chem. Int. Ed.* **2016**, *55*, 10287–10291
Angew. Chem. **2016**, *128*, 10443–10447

[1] D. M. Chapin, C. S. Fuller, G. L. Pearson, *J. Appl. Phys.* **1954**, *25*, 676–677. D. M. Chapin, C. S. Fuller, G. L. Pearson, US Patent 2 780-765, 5 February, **1957**.
[2] B. O'Regan, M. Grätzel, *Nature* **1991**, *353*, 737–740.
[3] R. Komiya, et al., in Technical Digest, 21st International Photovoltaic Science and Engineering Conference, Fukuoka, 2 C-5O-08 (**2011**).
[4] S. M. Feldt, E. A. Gibson, E. Gabrielsson, L. Sun, G. Boschloo, A. Hagfeldt, *J. Am. Chem. Soc.* **2010**, *132*, 16714–16724.
[5] A. Yella, H.-W. Lee, H. N. Tsao, C. Yi, A. K. Chandiran, M. K. Nazeeruddin, E. W.-G. Diau, C.-H. Yeh, S. M. Zakeeruddin, M. Grätzel, *Science* **2011**, *334*, 629–634.
[6] J.-H. Yum, E. Baranoff, F. Kessler, T. Moehl, S. Ahmad, T. Bessho, A. Marchioro, E. Ghadiri, J. E. Moser, C. Yi, M. K. Nazeeruddin, M. Grätzel, *Nat. Commun.* **2012**, *3*, 631.
[7] S. Mathew, A. Yella, P. Gao, R. Humphry-Baker, B. F. E. Curchod, N. Ashari-Astani, I. Tavernelli, U. Rothlisberger, M. K. Nazeeruddin, M. Grätzel, *Nat. Chem.* **2014**, *6*, 242–247.
[8] a) M. Urbani, M. Grätzel, M. K. Nazeeruddin, T. Torres, *Chem. Rev.* **2014**, *114*, 12330–12396; b) T. Higashino, H. Imahori, *Dalton Trans.* **2015**, *44*, 448–463.
[9] Y. Inokuma, J. H. Kwon, T. K. Ahn, M.-C. Yoo, D. Kim, A. Osuka, *Angew. Chem. Int. Ed.* **2006**, *45*, 961–964; *Angew. Chem.* **2006**, *118*, 975–978.
[10] A. Osuka, E. Tsurumaki, T. Tanaka, *Bull. Chem. Soc. Jpn.* **2011**, *84*, 679–697.
[11] T. Tanaka, M. Kitano, S.-Y. Hayashi, N. Aratani, A. Osuka, *Org. Lett.* **2012**, *14*, 2694–2697.
[12] Y. Inokuma, A. Osuka, *Chem. Commun.* **2007**, 2938–2940.
[13] M. Kitano, S. Hayashi, T. Tanaka, H. Yorimitsu, N. Aratani, A. Osuka, *Angew. Chem. Int. Ed.* **2012**, *51*, 5593–5597; *Angew. Chem.* **2012**, *124*, 5691–5695.
[14] A. Hagfeldt, G. Boschloo, L. Sun, L. Kloo, H. Pettersson, *Chem. Rev.* **2010**, *110*, 6595–6663.
[15] K.-J. Hwang, W.-G. Shim, S.-H. Jung, S.-J. Yoo, J.-W. Lee, *Appl. Surf. Sci.* **2010**, *256*, 5428–5433.
[16] C.-R. Lee, H.-S. Kim, I.-H. Jang, J.-H. Im, N.-G. Park, *ACS Appl. Mater. Interfaces* **2011**, *3*, 1953–1957.
[17] a) E. Ghadiri, N. Taghavinia, S. M. Zakeeruddin, M. Grätzel, J.-E. Moser, *Nano Lett.* **2010**, *10*, 1632–1638; b) J. R. Jennings, A. Ghicov, L. M. Peter, P. Schmuki, A. B. Walker, *J. Am. Chem. Soc.* **2008**, *130*, 13364–13372; c) J. R. Jennings, Y. Liu, Q. Wang, *J. Phys. Chem. C* **2011**, *115*, 15109–15120.
[18] G. Schlichthörl, N. G. Park, A. J. Frank, *J. Phys. Chem. B* **1999**, *103*, 782–791.
[19] M. Adachi, M. Sakamoto, J. Jiu, Y. Ogata, S. Isoda, *J. Phys. Chem. B* **2006**, *110*, 13872–13880.
[20] G. Schlichthörl, S. Y. Huang, J. Sprague, A. J. Frank, *J. Phys. Chem. B* **1997**, *101*, 8141–8155.

Received: May 6, 2016
Revised: June 17, 2016
Published online: August 2, 2016

